Supporting Information

Controllable Curvature from Planar Polymer Sheets in Response to Light

Amber M. Hubbard†, Russell W. Mailen†, Mohammed A. Zikry, Michael D. Dickey, and Jan Genzer**

Amber M. Hubbard, Prof. Michael D. Dickey, Prof. Jan Genzer
Department of Chemical and Biomolecular Engineering NC State University Campus Box 7905
Raleigh, NC 27695-7905 U.S.A.

Russell W. Mailen, Prof. Mohammed A. Zikry
Department of Mechanical and Aerospace Engineering NC State University Campus Box 7910
Raleigh, NC 27695-7910 U.S.A

† Equal contributions to the paper; authors listed in alphabetical order.

Figure S1A depicts the sample fabrication process. Pre-strained polystyrene sheets, commercially available as Grafix® shrink film, were printed with black ink using a desktop, inkjet printer. The patterns were cut from the sheet using scissors and placed in the center of a hot plate set to 90°C.[1] An IR light stationed ~ 5 cm above the surface of the sample was then turned on, and the subsequent sample shrinkage resulted from localized absorption of the IR light by the patterned regions.

The folded samples were imaged with a Canon EOS Rebel T3 DSLR camera from the top down after removal of the IR light stimulus (see far right image in **Figure S1A**). These images were processed by an edge detection algorithm in MATLAB. **Figures S1B,C** depict an example inputted image and the algorithm output, respectively. For demonstrative purposes the used images are of a hen-and-chicks succulent plant, part of the Crassulaceae family. This plant exhibits multiple radii of curvature in various portions of the structure, as depicted by the two red circles outlined on **Figure S1C**.

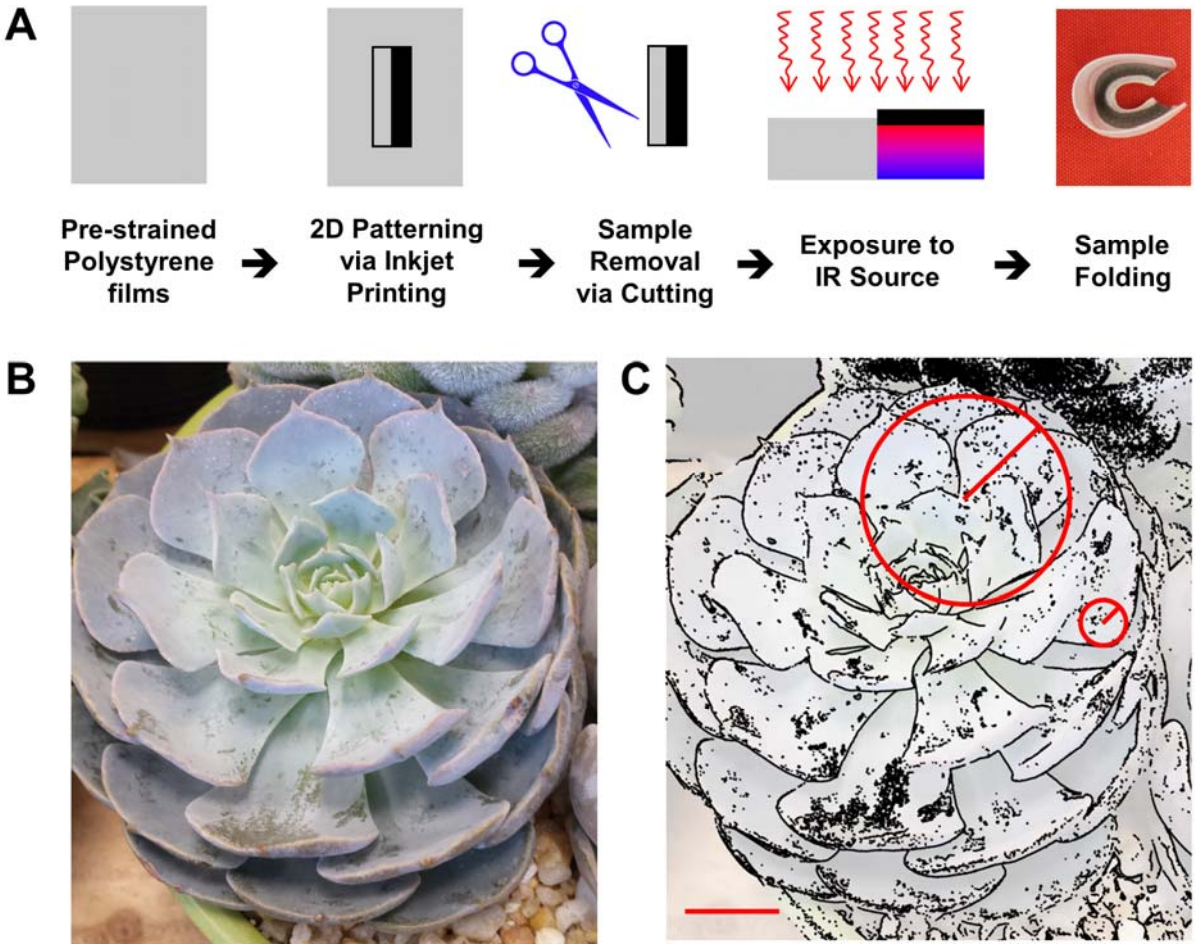

Figure S1. (A) A step-by-step process depicting the experimental sample preparation and recovery processes. The sample designs were printed onto the polystyrene sheets and cut out using scissors. The samples were exposed to an IR source which locally heats the sample and causes it to shrink and deform. (B) A sample image of a plant with multiple different radii of curvature that was analyzed by a MATLAB edge detection algorithm with the resulting image (C) highlighting two distinct R_c (depicted by red circles) found throughout the structure. The scale bar is 25 mm.

The amount of IR energy absorption depends upon the distribution and darkness of ink placed onto the sample. **Figure S2A** shows the relationship between ink darkness, temperature, and IR absorption. The top row of **Figure S2A** depicts a linear gradient in ink darkness across the length of the sample, identical to the pattern shown in **Figure 5B**. The second image shows temperature results captured with an FLIR® SC300 Series camera. This image is scaled to the same size as the ink pattern and is aligned with a plot of absorption and surface temperature

shown in the bottom row of **Figure S2A**. At 100% darkness, the ink coverage on our samples is never truly 100% due to limitations in the printing capabilities of an inkjet printer. Instead, the maximum ink coverage was experimentally found to reach a maximum of ~ 70% coverage which was then used to normalize our nominal ink density values. The normalized absorption values were collected via Ultraviolet/Visible Spectroscopy and recorded as an average absorption percentage across the 400 – 800 nm wavelength range for 11 sample sets (ranging from 0 % to 100 % nominal ink density). These results were gathered in triplicate. Further information regarding the absorption of IR light by the inked surface has been previously reported.[2] The surface temperature values correspond to data gathered in the ExamineIR™ software with the use of the thermal camera. To demonstrate the agreement of this heating behavior with computational results, a sample structure is depicted in **Figure S2B** which corresponds to the anticlastic structure seen in **Figure 2**. The regions with ink patterning are heated to temperatures exceeding the activation temperature ($T_a \sim T_g$).

Videos S1-S2, available online, demonstrate the recovery response of the synclastic and anticlastic experimental samples, respectively, from **Figure 2** in real time. The red lighting seen in these videos is due to the IR lamp and the silver background is aluminum foil placed over the face of the hot plate. **Video S3**, available online, demonstrates a sample with the direct mechanism of curvature (a gradient in ink darkness) for the 3:1 aspect ratio substrate in real time.

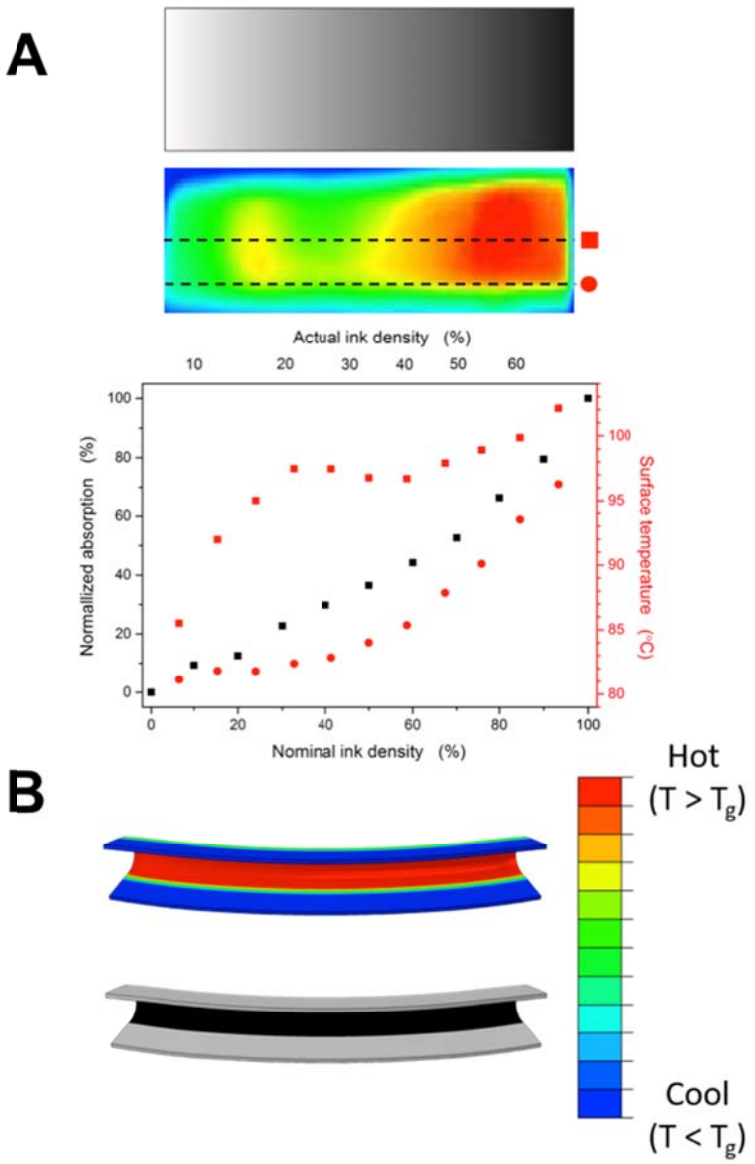

Figure S2. A graphical and visual depiction of how surface temperature and normalized IR absorption increases with nominal and actual ink density for experimental (A) and computational (B) results. The temperature values used within the graph are directly correlated to the values on the thermal image (A). The dashed black lines overlaid on the IR image visually depict that the surface temperature values were recorded at the centerline (squares) and lower edge (circles). The lower image in B represents the ink pattern where the grey regions are unpatterned and the black regions indicate ink coverage.

In **Figure 4**, samples that reflect the indirect mechanism of curvature are shown for three aspect ratios. A similar study was performed for the direct curvature mechanism samples presented in **Figure 5A-C**. The experimental results for the three aspect ratios are shown in

Figure S3. Similar to the indirect curvature samples, samples with higher aspect ratios had a larger overall deformation with similar radii of curvature due to the increase in the overall length of material. A similar trend was observed as the aspect ratio was changed for each pattern.

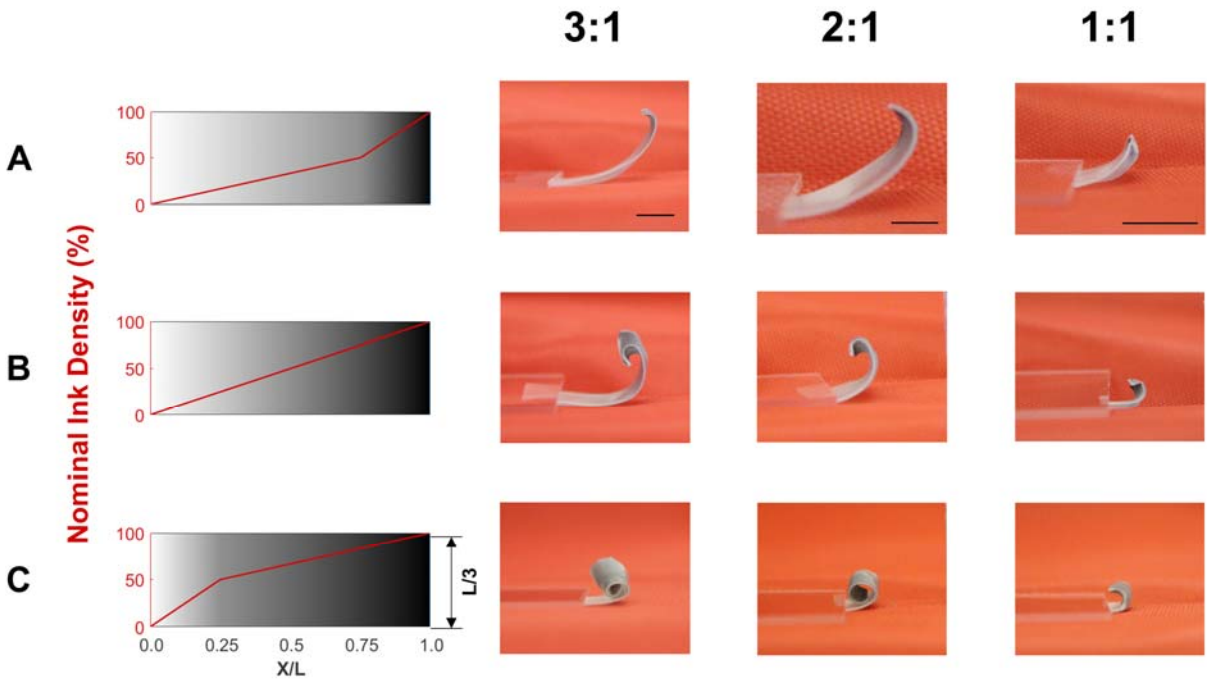

Figure S3. An illustration of the effects of changes to the sample aspect ratio while maintaining the designated gradient pattern. Samples became more curved with the increase in aspect ratio, while the same general trend was observed for each gradient ink pattern. The scale bar is 5 mm for 3:1 aspect ratio samples and 10 mm for the 2:1 and 1:1 aspect ratio samples.

A serial sectioning technique (*cf.* **Figure S4A**) was employed to demonstrate the excellent qualitative agreement between the computational and experimental results. The samples were painted for increased contrast and are imbedded within a clear polyester casting resin. The resulting round, puck-like structure was milled through in ~ 0.5 mm segments and digitally imaged between each milling step. The MATLAB edge detection algorithm, discussed for **Figure S1B,C**, was applied to each image, and data points were gathered between each segment to generate a complete digital, 3D point cloud for the experimental samples as seen in **Figures S4B,C**. Note that the milling marks can still be seen for the outputted image of the edge

detection algorithm, but only points on the sample were selected manually to produce the final 3D representation. A gradient in color was assigned to the point cloud as a visual representation for changes in height. The computational model was overlaid in black onto the experimental point cloud and demonstrates the excellent agreement. **Videos S4-S5** available online show the point cloud results for the bordered (indirect curvature) and gradient (direct curvature) samples, **Figure 6B** and **C** respectively, from various angles for increased clarity.

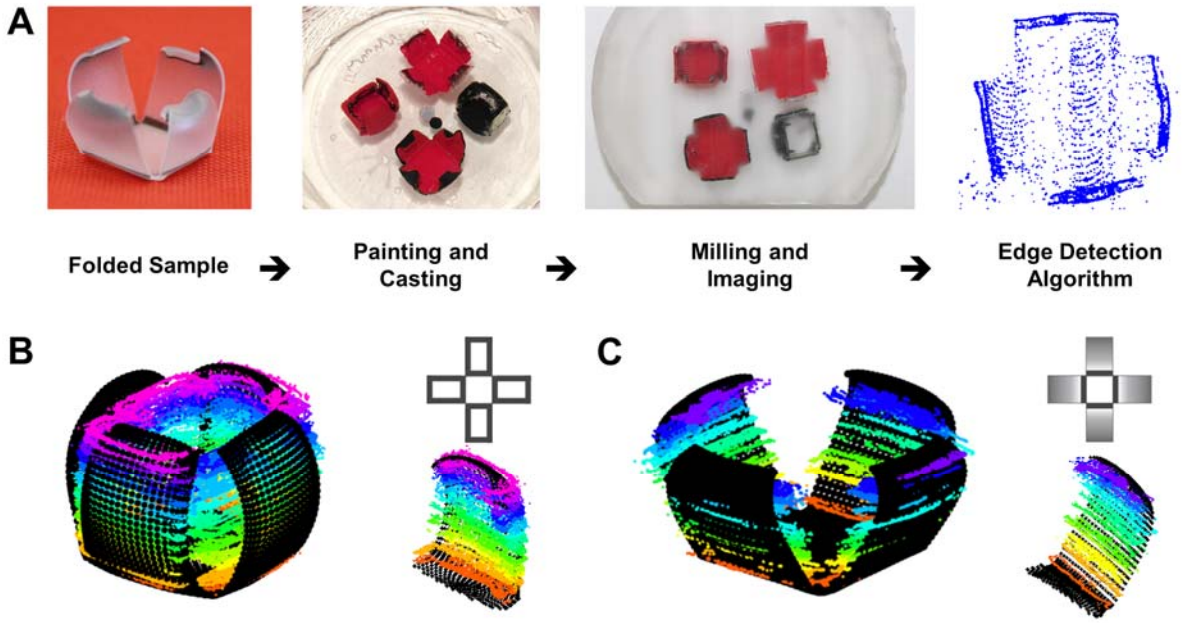

Figure S4. Serial section process used to obtain the digital, 3D point cloud of the bio-inspired structures. (A) The samples were painted, casted, milled in ~ 0.5 mm segments, and digitally imaged to acquire the necessary data points. The final point cloud can be seen for both the (B) indirect and (C) direct mechanism of curvature. The gradient in color corresponds to changes in height while the black data points represent the computational results.

The radius of curvature (R_c) in quantitatively analyzed samples was calculated by selecting three points from the outputted MATLAB edge detection algorithm graph, similar to the plot seen in **Figure S1C** and depicted in **Figure 7A**. The coordinates x_i and y_i for each of the three data points were entered into **Equations S1 – S4** below

$$Slope = \frac{\Delta y}{\Delta x} \quad \textbf{(S1)}$$

$$X_C = \frac{m_1 m_2 (y_1 - y_3) + m_2 (x_1 + x_2) - m_1 (x_2 + x_3)}{2(m_2 - m_1)} \quad \textbf{(S2)}$$

$$Y_C = -\frac{1}{m_1}\left(X_C - \frac{x_1 + x_2}{2} \right) + \left(\frac{y_1 + y_2}{2} \right) \quad \textbf{(S3)}$$

$$R_C = \sqrt{(x_1 - X_C)^2 + (y_1 - Y_C)^2} \quad \textbf{(S4)}$$

where m_1 and m_2 are the slopes between the three chosen locations. The pertinent variables are visually defined in **Figure S5**. The R_c was calculated for both the computational and experimental samples, averaged across ~ 16 panels for each sample design. As seen in **Figure 7**, there is excellent quantitative agreement between the computational and experimental results with some slightly elevated standard deviation values due to previously mentioned experimental factors.

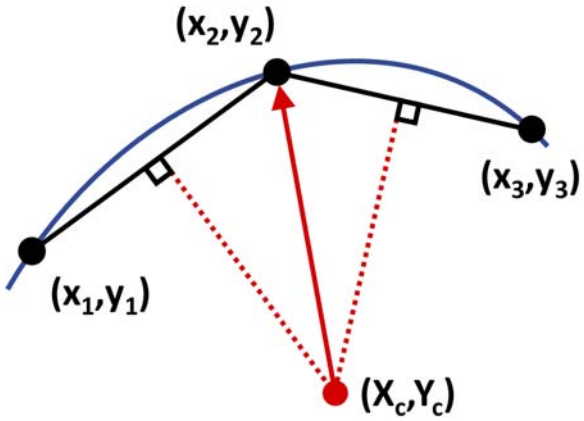

Figure S5. Schematic defining variables in **Equations S1-S4**.

Supporting Information References:

1 Ying Liu, Julie K. Boyles, Jan Genzer and Michael D. Dickey, *Soft Matter*, 2012, **8**, 1–6.

2. Y. Liu, R. Mailen, Y. Zhu, M. D. Dickey and J. Genzer, *Phys. Rev. E*, 2014, **89**, 042601.